JOURNAL OF MATERIALS SCIENCE 29 (1994) 5071–5077

The δ-Al_2O_3 (Saffil) fibre degradation during infiltration with MgLi alloy

S. KÚDELA, V. GERGELY, A. SCHWEIGHOFER
Institute of Materials and Machine Mechanics, Slovak Academy of Sciences, 836 06 Bratislava, Slovakia

S. BAUNACK, S. OSWALD, K. WETZIG
Institute for Solid State and Materials Research, Institute for Solid State Analytics and Structural Research, D-01171 Dresden, Germany

The chemical and phase transformations of δ-Al_2O_3 (Saffil) fibres during their infiltration with Mg–8 wt% Li were studied by scanning and transmission electron microscopy, Auger electron spectroscopy, secondary ion mass spectrometry and X-ray diffraction methods. The infiltration experiments were carried out in autoclave under argon pressure at temperatures of 883–908 K and contact times of 4–30 s as well as at 918 K/420 s. During the course of infiltration, lithium penetrates the Saffil fibres and this process is accompanied by the gradual transformation of the tetragonal δ-Al_2O_3 lattice towards the cubic spinel $LiAl_5O_8$ compound, where part of the Li^+ ions is probably substituted by Mg^{2+}. No remarkable interfacial zone at the fibre/matrix interface was observed; however, the Saffil fibres became brittle which had been manifested by the occurrence of fragmentation on the metallographically treated fibre cross-sections. The tensile strength (maximum 220 MPa) of the corresponding metal matrix composite clearly decreased with increased infiltration time.

1. Introduction

The Saffil (trademark of ICI Americas, Inc. Wilmington, DE) fibre preform infiltration with liquid metals represents an economical method of metal matrix composites (MMCs) manufacture, especially on a light alloys basis. The Saffil fibres consisting of polycrystalline δ-Al_2O_3 as a dominant phase and a small amount of SiO_2 are characterized by high mechanical parameters which allow them to have a considerable reinforcing effect in their applications in MMCs, provided degradation phenomena in a fibre/matrix interaction can be maintained at a minimum level.

Magnesium–lithium alloys, as the lightest metallic structural material (1.4–1.6 $g\,cm^{-3}$) would be very attractive candidates for reinforcement with high-strength or high-modulus fibres, because these MMCs can be prepared with high strength-to-density ratios. The Saffil/MgLi is undoubtedly a very promising combination from this point of view; however, problems arise with the compatibility of the Saffil fibres with the MgLi matrix, especially for high lithium contents.

A preliminary analysis has suggested that the Al_2O_3–(SiO_2)–Mg–Li system is thermodynamically unstable. If we focus only on the Al_2O_3 component of Saffil fibres, the reductive reaction can occur at infiltration temperatures (about 900 K), leading to the oxides (MgO, Li_2O), aluminates ($LiAlO_2$, Li_5AlO_4) and spinels ($MgAl_2O_4$, $LiAl_5O_8$) formation [1, 2] which may have a negative influence on the Saffil fibre properties.

The only published report concerning the interaction of Saffil fibres with MgLi alloys in MMC manufacturing is that of Mason *et al.* [3] who studied the compatibility of Saffil fibres with the Mg–12 wt % Li alloy in the pressure infiltration process, and found that Saffil fibres became brittle upon interaction with the matrix, which the authors explained by lithium penetration along δ-Al_2O_3 crystallite grain boundaries. They also observed good fibre/matrix interfacial bonding and stated that only SiO_2 binder reacted extensively with Mg12Li alloy.

The present study was aimed to obtain some picture of the chemical processes which took place in Saffil fibres during their infiltration by the Mg–8 wt % Li alloy in context with structure and strength characteristics of the corresponding Saffil/Mg8Li MMC. The experiments were carried out in such a way that a series of MMC samples, representing different component interaction stages, was prepared by means of pressure infiltration technology and, subsequently, the chemical and phase composition changes of Saffil fibres, which occurred during their contact with liquid Mg8Li alloy, were investigated by means of scanning and transmission electron microscopy (SEM, TEM), Auger electron spectrometry (AES), secondary ion mass spectroscopy (SIMS) and X-ray diffraction (XRD) methods.

2. Infiltration experiments

In performing infiltration experiments, a Saffil RF-grade fibre preform consisting predominantly of short

0022–2461

planar randomly oriented polycrystalline δ-Al_2O_3 fibres ($\approx$20 vol %) and SiO_2 binder ($\approx$4 wt %) was used. The Saffil fibres are characterized by a mean diameter of 3–4 μm and mean length about 0.5 mm, whereas the tensile strength of fibres is R_m = 2000 MPa and Young's modulus E = 320 GPa [4]. The δ-Al_2O_3 crystallites are stabilized by 3–4 wt % SiO_2 and individual fibres are also covered with a colloid silica film. The mean δ-Al_2O_3 crystallite size is about 50 nm [5].

The Saffil fibre preform was infiltrated with a Mg–8 wt % Li alloy which had been prepared using magnesium (purity 99.99%) and lithium (purity 99.5%) as starting raw materials by casting under argon pressure (purity 99.999%). As follows from the binary Mg–Li diagram, the Mg8Li alloys should exhibit in the solid state, a two-phase structure (hcp–bcc) with the liquidus temperature of 860 K (eutectic temperature).

The infiltration experiments were performed in a laboratory autoclave by complete submersion of the Saffil fibre preform into a liquid metal bath (temperature T_i) in a vacuum of $P_v \sim 10$ Pa and successive action of the inert gas pressure. A preform with the dimensions $37 \times 10 \times 3$ mm^3 was preheated to the temperature of $T_p \approx 470$ K before submersion took place. The diagram of the temperature and pressure operation during the infiltration cycle is given in Fig. 1.

The infiltration time $t = t_2 - t_1$ was defined as the interval between the onset of pressure medium inflow (time t_1) and the moment the infiltrated preform was withdrawn (time t_2). The gas pressure during infiltration increased continuously from the vacuum P_V at the time t_1 to the value P_i at the time t_2. Values of T_i were gradually set to 878, 888, 898, 908 K and contact times were chosen from 4–30 s.

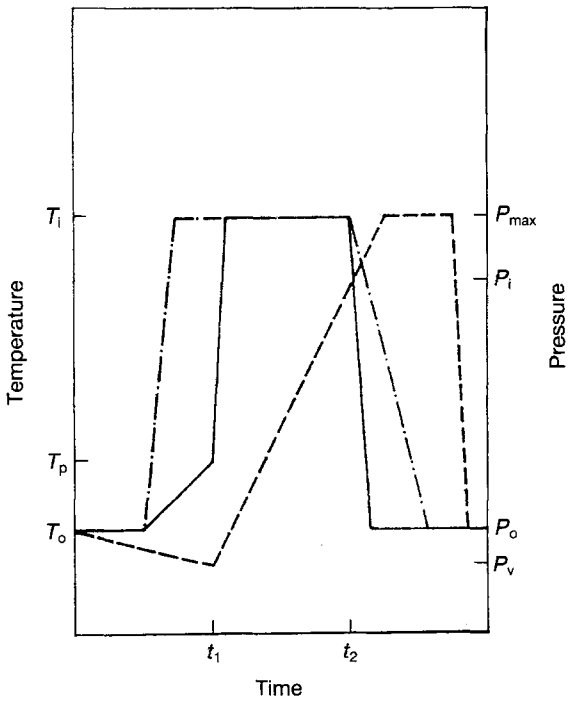

Figure 1 Diagram of the temperature and pressure operation during an infiltration cycle. (——) Sample temperature, (–·–) liquid metal temperature, (– – –) gas pressure.

3. Results

3.1. Microstructure

Typical micrographs of both longitudinal and transverse MMC sections are shown in Fig. 2a and b. Detail of Saffil fibre layout in a two-phase Mg8Li matrix is shown in Fig. 3. Fig. 4 shows that no reaction interlayer was observed at the fibre/matrix interface within the interval of reaction parameters under investigation. Fine cubic crystals, which were identified as MgO from the electron diffraction patterns (TEM), were observed only in localities of the silica binder, frequently in contact with Saffil fibres.

Extensive Saffil fibre fragmentation was observed on some of the metallographically treated sections, obviously as a result of the grinding and polishing operations (Fig. 5). The extent of fragmentation correlated with increasing infiltration temperature and time. Saffil fibres which had been extracted from the MMCs by selective dissolution of the Mg8Li matrix (CH_3OH + 10%Br solution) displayed no damage (Fig. 6).

3.2. X-ray diffraction analysis (XRD)

Using a bromine–methanol mixture as solution agent, Saffil fibres were extracted from the MgLi matrix and studied by X-ray phase analysis. Diffraction patterns were taken using Siemens D 500 apparatus with FeK_α radiation (Debye powder method).

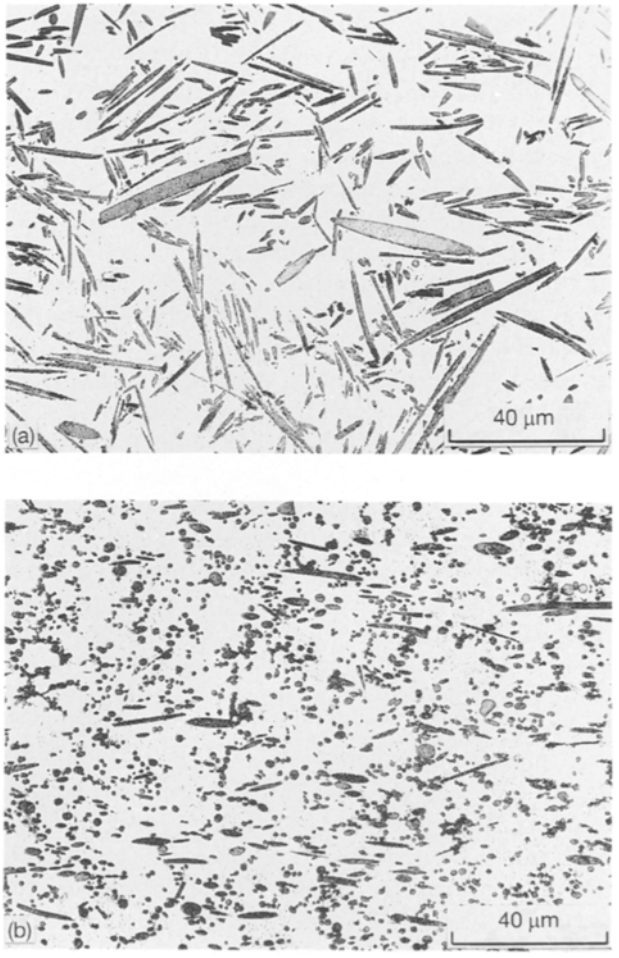

Figure 2 Typical optical micrographs of the Mg8Li/Saffil MMC sample: (a) longitudinal section, (b) transverse section.

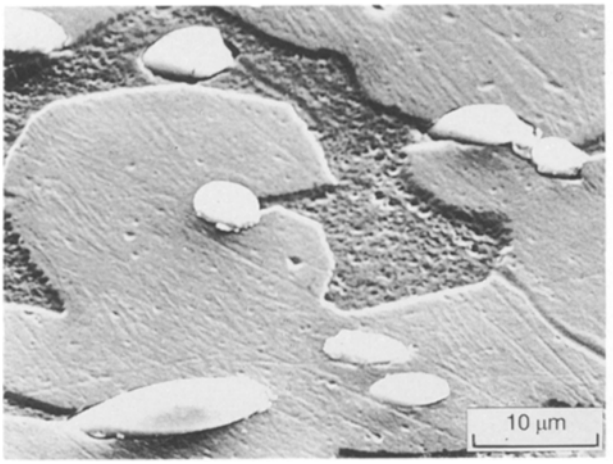

Figure 3 Scanning electron micrograph of a polished transverse section of Mg8Li/Saffil MMC (888 K/15 s) showing Saffil fibre layout in a two-phase Mg8Li matrix. Etching agent: 10% CH_3COOH solution in *i*-propanol.

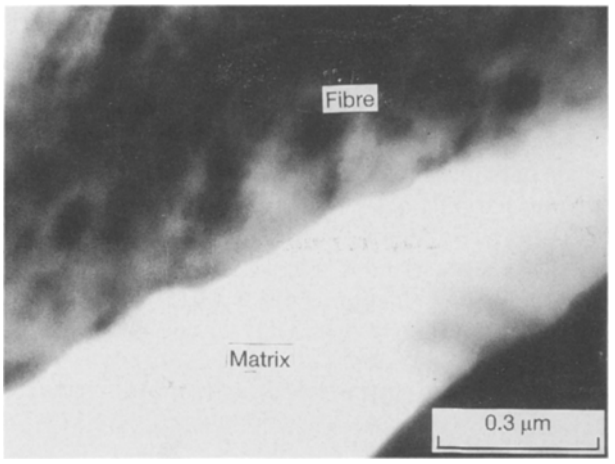

Figure 4 TEM bright-field micrograph of Saffil fibre/matrix boundary region in MMC infiltrated at 888 K/10 s.

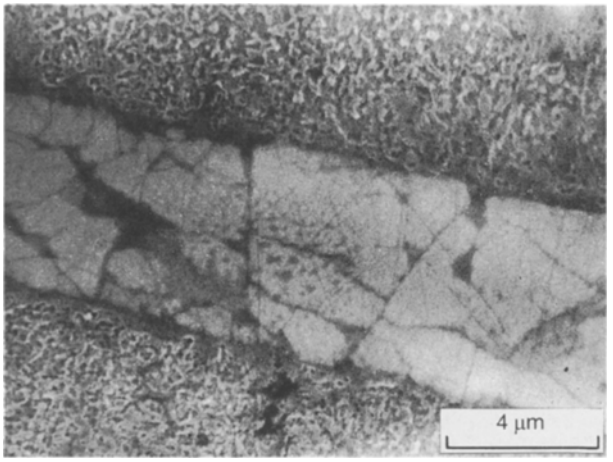

Figure 5 Scanning electron micrograph of polished longitudinal section of MMC infiltrated at 908 K/30 s showing the Saffil fibre fragmentation.

The phase composition of Saffil fibres was changed owing to their interaction with the Mg8Li matrix, which is shown by the diffraction patterns in Fig. 7. Fig. 7a corresponds to the virgin Saffil fibres, whereas

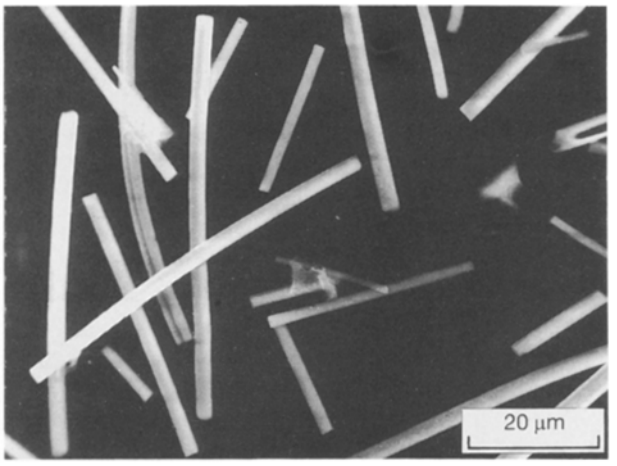

Figure 6 SEM image of Saffil fibres extracted from MMC (908 K/15 s).

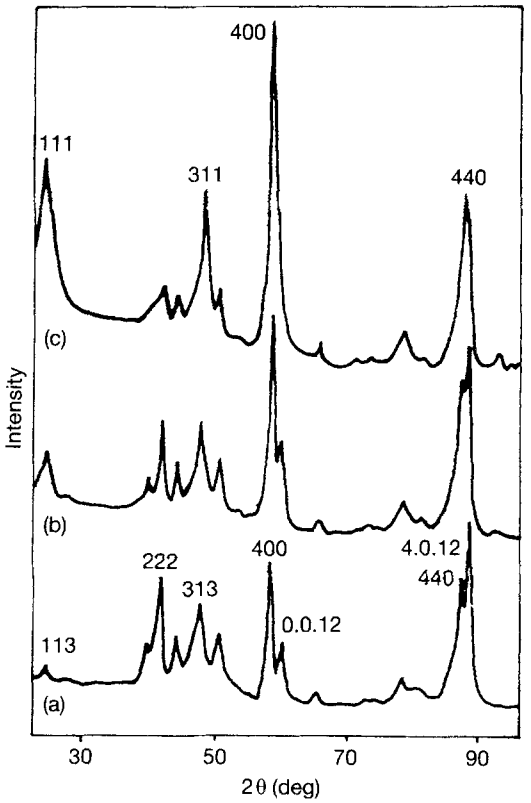

Figure 7 X-ray diffraction patterns taken from (a) virgin Saffil fibres, (b) Saffil fibres extracted from MMC (888 K/10 s), (c) Saffil fibres extracted from MMC (918 K/420 s).

Fig. 7b was taken from extracted fibres of the MMC specimen (888 K/10 s). Fig. 7c was also taken from the extracted fibre specimen (918 K/420 s) as an extreme reaction condition case.

The δ-Al_2O_3 tetragonal phase with cell parameters $a = b = 0.7953$ nm, $c = 2.3512$ nm, and also a small quantity of the cubic γ-Al_2O_3 were identified in the virgin Saffil fibres. The diffraction patterns (a–c) are very alike, although there is obviously a gradual confluence of the reflections 400/0012 and 440/4012, and their relative intensities change as well. These attributes are typical for the gradual transformation of δ-Al_2O_3 tetragonal lattice to the cubic spinel lattice [6]. In connection with a higher crystallographic symmetry of the forming spinel lattice, high

index planes decay and the remaining peaks can be simply reindexed to the spinel lattice. Obviously, in the diffraction patterns, a gradual decomposition of the δ-Al_2O_3 superlattice into individual spinel blocks with a cell parameter of $a = 0.7934$ nm can be observed. This value is relatively close to the cell parameter reported for the $LiAl_5O_8$ spinel ($a = 0.7908$ nm for the ordered form and $a = 0.7925$ nm for the disordered form, respectively [7]). However, the well-developed diffraction patterns corresponding to this spinel compound were obtained only under extreme infiltration conditions (918 K/420 s). Under the range of infiltration conditions used, (878–908 K/4–30 s), the transformation of δ-Al_2O_3 towards the spinel compound has not yet been finished completely, as suggested by the split existence of the pairs of reflections 400/0012 and 440/4012.

3.3. Auger electron spectroscopy (AES)

Auger electron spectra were taken at the primary electron beam energy of 3 keV and beam current of 30 nA, by the Perkin–Elmer PHI 660 SAM microprobe (the lateral resolution at the conditions mentioned is about 300 nm) on metallographically treated areas after short sputtering (argon ions of 4 keV) from the Mg8Li matrix locality, as well as the central part of the Saffil fibre cross-section. Table I lists the energies of the Auger peaks in the $dN(E)/dE$ mode in both Saffil fibres and matrix (sample 908 K/30 s). The corresponding part of the $dN(E)/dE$ spectrum in the low-energy region (20–70 eV) is shown in Fig. 8.

First, it must be stated that direct lithium identification by AES was not possible here, because the peaks at 34 and 45 eV can refer to both magnesium and lithium. Secondly, the peaks at 34.5 and 66.5 eV, as well as 1187 eV (marked by * in Table I) were influenced by the electron beam-induced dissociation of the corresponding oxides.

The following comments can be made on the obtained AE spectra.

(i) Magnesium was detected in the Saffil fibres cross-section. An Auger map ($E = 1186$ eV) showed that magnesium was distributed on the Saffil fibre cross-sectional area quite homogeneously. It should be noted that no magnesium peak was observed in Saffil fibre cross-sections if the Saffil fibres had been infiltrated with pure magnesium.

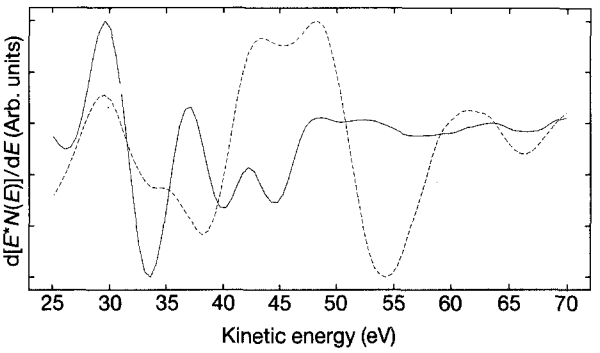

Figure 8 AES peaks in the low-energy region taken from the central part of (– – –) a Saffil fibre cross-section, as well as from (——) the Mg8Li matrix (908 K/30 s).

(ii) The Al_2O_3 peaks in Saffil fibres display in the low-energy region a shift $\Delta E \approx +3.5$ eV with respect to the reference data. This can be interpreted as a chemical shift; however, a shift from charging of the fibre cannot be excluded. On the other hand, the virgin Saffil fibres impressed into an inactive metallic matrix (indium) exhibit AE peaks coinciding quite exactly with the reference data for Al_2O_3, whereas measurements of Saffil fibres in pure magnesium suffered from sample charging.

(iii) In the Saffil fibres cross-section, metallic aluminium was detected (at 67 eV) which might be a result of the reductive reaction of the δ-Al_2O_3 component.

3.4. Secondary ion mass spectrometry (SIMS)

The same extracted fibres which had been subjected to the X-ray diffraction analysis were also studied by SIMS combined with a gradual sputtering (Ar^+ ions). The SIMS experiments were carried out in such a way that at first the studied fibres were mechanically impressed into an indium foil (purity 99.99%) and subsequently an area of 30×30 μm^2 containing extracted fibres and/or virgin Saffil fibres was analysed with a maximum sputtering time of 30 min. The extension of the sputtering time beyond 30 min was accompanied by extensive charging effect and therefore the depth profiles presented represent only the peripheral region

TABLE I Kinetic energies of Auger electrons

AE kinetic energy (eV)				Element or compound (Auger transition)
Fibre in In	Fibre in Mg8Li	Mg8Li Matrix	Reference data	
–	34.5*	34.0	34.0 [8]	Li(KVV), Mg(LVV)
35.0	38.5	–	35.0 [8]	Al_2O_3(LVV)
–	–	40.0	40.0 [10]	Li_2O(KVV)
–	45.5	45.0	43.0; 45.0 [8]	LiF(KVV), Mg(LVV)
51.5	54.5	–	51.0 [8]	Al_2O_3(LVV)
–	67.0*	–	68.0 [8]	Al(LVV)
–	1182.0	–	1174.0 [9]	MgO(KLL)
–	1187.0*	1186.0	1186.0 [8, 9]	Mg(KLL)
1388.0	–	–	1378.0 [8, 9]	Al_2O_3(KLL)
–	1391.0	–	1396.0 [8, 9]	Al(KLL)

* Peaks affected by electron beam-induced decomposition of oxides.

(about 100 nm) of the studied Saffil fibres. The depth profiles were measured using an ion microprobe mass analyser (IMMA from Applied Research Laboratories).

The SIMS experiments were aimed at the Li/Al as well as the Mg/Al concentration ratio determination in the oxide fibres studied because these elements should occupy the cation sites in the spinel lattice, in accordance with X-ray diffraction results. Thus, the obtained concentration depth profiles of lithium, magnesium and aluminium were normalized to the sum of these signals. For calculation, only semiquantitative sensitivity factor values were used. Therefore, the obtained concentration data are presented as approximate ones. Moreover, the SIMS results can be affected by the ion migration occurring at the analysed surfaces due to the surface charging effect [11].

Fig. 9 shows the concentration depth profiles of aluminium, lithium and magnesium obtained from different treated Saffil fibres impressed in indium foil. For the fibres extracted from the MMC 918 K/420 s (Fig. 9d) an Li/Al ratio of approximately 1:4 was found which we take for a nearly stoichiometric $LiAl_5O_8$ composition (Li/Al ratio 1:5) in semiquantitative approach. On the other hand, the fibres extracted from the MMC 888 K/10 s (Fig. 9c) exhibited an Li/Al ratio of 1:10 only.

The concentration depth profile taken from fibres infiltrated with pure magnesium is shown (Fig. 9b) and it is evident that the magnesium concentration is about the same here as was detected in virgin Saffil fibres (Mg/Al ratio less than 0.01). A rather enhanced magnesium concentration was observed only in the fibres extracted from MMC 918 K/420 s (Mg/Al ratio above 0.01) with some tendency to increase with increasing sputtering time.

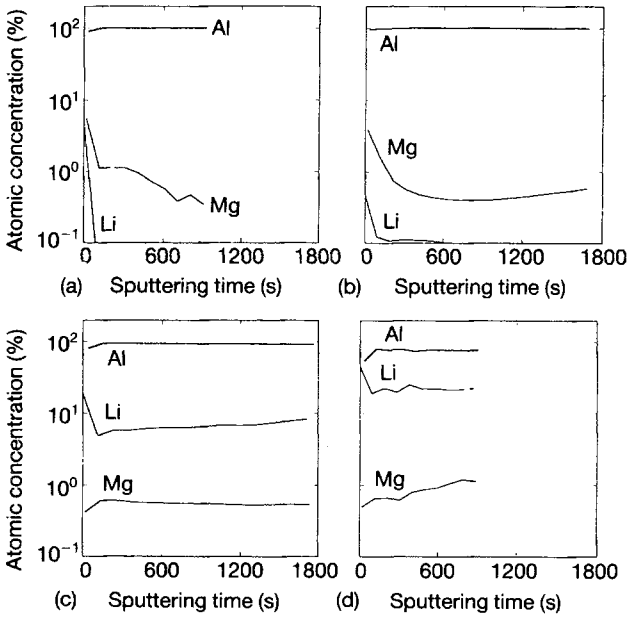

Figure 9 SIMS depth profiles of lithium, magnesium and aluminium in Saffil fibres impressed in indium foil: (a) virgin Saffil fibres, (b) Saffil fibres extracted from the magnesium matrix, (c) Saffil fibres extracted from the Mg8Li matrix (888 K/10 s), (d) Saffil fibres extracted from the Mg8Li matrix (918 K/420 s).

3.5. Mechanical properties

In Table II, infiltration process variables, T_i, P_i, t, and tensile strength values, R_m, are given as well as Young's modulus, E, of the corresponding MMC. The tensile test specimens were flat parallel to the planar fibre layout (see Fig. 2a). The influence of infiltration temperature, T_v, and contact time, t, upon R_m values of the prepared samples is shown in Fig. 10. The tensile strength of the as-cast Mg8Li alloy was $R_m = 100$ MPa and the Young's modulus $E = 42$ GPa.

It is evident that the strength maximum of $R_m = 220$ MPa is reached at 898 K, and from a certain value the infiltration temperature begins to influence R_m values negatively. The increased contact time leads to a decrease in R_m values in the studied infiltration variables range. The Young's modulus, E (three-point bending test), is less sensitive to infiltration parameters; however, a negative influence of contact time prolongation upon E values is obvious.

Macrodefects (poorly infiltrated Saffil preform localities) were observed in some MMCs. It appears that the number of macrodefects correlates with R_m values, when their occurrence exhibits a minimum for samples infiltrated at 898 K (strength maximum). In a region of low infiltration temperatures (below 898 K) it may be caused by an insufficient fluidity of penetrated Mg8Li liquid alloy.

On the other hand, in a region of higher temperatures (above 898 K) the reduced alloy fluidity may be a result of lithium removal from the MgLi alloy caused by its chemical reaction with Saffil fibres. The tensile strength, R_m, of prepared MMC clearly decreased with increasing infiltration time at a given infiltration temperature, which could be considered to

TABLE II Mechanical properties of prepared MMC

T_i (K)	t (s)	P_i (MPa)	E (GPa)	R_m (MPa)
878	15	3.8	65	109
878	30	5.0	58	91
888	4	1.0	54	113
888	15	4.0	58	100
898	4	1.0	66	220
898	15	3.8	56	155
898	30	5.0	51	150
908	4	1.0	58	145
908	15	4.0	66	117
908	30	5.0	50	72

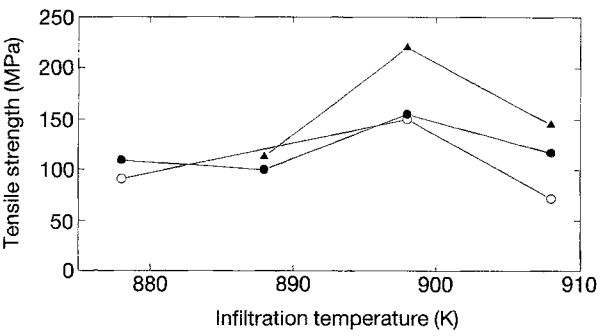

Figure 10 Diagram of tensile strength, R_m, versus infiltration temperature, T_i, at different infiltration times: (▲) 4s, (●) 15s, (○) 30s.

be a result of chemical and phase changes of Saffil fibres owing to their interaction with Mg8Li matrix. However, the reinforcing effect obtained at optimal infiltration conditions was at least comparable with that reached at Saffil/magnesium MMC [12, 13].

4. Discussion

As expected, the interaction of Saffil fibres with Mg8Li alloy during the infiltration process was strongly affected by the presence of lithium in the infiltrating alloy. The δ-Al_2O_3 decomposition and gradual formation of spinel compound accompanied by lithium and magnesium penetration into the Saffil fibre interior were observed, in contrast to the results obtained in the study of interaction of Saffil fibres with a pure magnesium. Hallstedt *et al.* [14] reported that during infiltration of Saffil fibres with pure magnesium the reaction between amorphous silica binder and liquid magnesium was the only important one, leading to an almost complete binder transformation to a very fine-grained magnesia and Mg_2Si particles which precipitated upon cooling. Despite the strong affinity between magnesium and oxygen, no remarkable interaction between δ-Al_2O_3 and liquid magnesium had been observed which the authors explained by the exceedingly low diffusivity of aluminium through the surface layers of $MgAl_2O_4$ and MgO.

The tetragonal δ-Al_2O_3 lattice is a superstructure of three γ-Al_2O_3 spinel cells ($a = 0.7943$ nm, $c = 2.350$ nm [15]), i.e. it is a defect lattice having some vacant cation sites because of electric charge compensation. Although the positions of vacancies in δ-Al_2O_3 have not been precisely defined, δ-Al_2O_3 has been assigned octahedral vacancies by analogy with the similar γ-Fe_2O_3 phase [16]. Thus, the spinel cell in the δ-Al_2O_3 superlattice can be expressed by the formula $Al_8[Al_{40/3}\square_{8/3}]O_{32}$, where the terms in brackets represent octahedrally coordinated ($z = 6$) cations or vacancies (denoted by $\square$). Such a structure is metastable, and on heating it can be transformed into thermodynamic equilibrium represented by α-Al_2O_3.

tendency towards octahedral co-ordination (Li^+, Na^+), into the δ-Al_2O_3 lattice, the cation vacancies can be effectively filled, provided that the cation distribution in the O^{2-} sublattice is close to the very stable 8(T)–16(O) spinel cation arrangement (T, tetrahedral cations; O, octahedral cations). The tetragonal δ-Al_2O_3 superlattice becomes unstable in this way and its decomposition into individual spinel blocks can occur.

The stabilizing effect of Li^+ cations on the γ-Al_2O_3 spinel structure has also been observed experimentally during calcination of the γ-Al_2O_3 substrate by lithium salts and subsequent thermal treatment [17]. In this process the Li^+ cations penetrated the γ-Al_2O_3 lattice, occupying octahedrally coordinated defective cation sites, and resulting in an enhanced thermal stability of spinel alumina, so that its transformation towards α-Al_2O_3 is completely inhibited [18].

In the X-ray diffraction pattern (Fig. 7), a gradual decomposition of the tetragonal δ-Al_2O_3 into spinel cells can be observed, maintaining the f c c oxygen anion sublattice. Obviously, this phase transformation is connected with lithium penetration into the Saffil fibre's interior and its incorporation into the δ-Al_2O_3 lattice by a similar mechanism to that mentioned above. The lithium penetration was experimentally confirmed by SIMS to the depth of ~ 100 nm; however, the penetration depth seems to be much larger, as indicated by the AES detection of metallic aluminium in central parts of Saffil fibre cross-sections. It can be assumed that mobile lithium atoms diffuse during the infiltration process down the δ-Al_2O_3 grain boundaries (enriched by SiO_2) with subsequent Li_2O formation around δ-Al_2O_3 crystallites by the chemical reactions

$$Al_2O_3 + 6Li = 3Li_2O + 2Al \quad (1)$$

$$SiO_2 + 4Li = 2Li_2O + Si \quad (2)$$

The Li^+ cations then penetrate the δ-Al_2O_3 lattice, gradually occupying the octahedral vacant sites according to the scheme $Al^{3+} + 2\square = 3Li^+$, which can be expressed by the stoichiometric equation (calculated for one spinel cell)

$$xLi^+ + Al_8[Al_{40/3}\square_{8/3}]O_{32} = Al_8[Al_{40-x/3}\square_{8-2x/3}Li_x]O_{32} + x/3Al^{3+} \quad (3)$$

As seen, the reorganization of cation sites occurs in octahedral positions exclusively, leading to the inverse spinel $LiAl_5O_8$ formation in the final stage ($x = 4$).

In Saffil fibres infiltrated with Mg8Li alloy, some amount of magnesium has also been detected. Most probably, the Mg^{2+} cations are incorporated into the $LiAl_5O_8$ spinel formed by an ion exchange, $Li^+ + Al^{3+} = 2Mg^{2+}$, leading to the mixed spinel compound $Al_8[Al_{12-x}Li_{4-x}Mg_{2x}]O_{32}$ formation. The Mg^{2+} cations cannot compete with Li^+ in incorporation into the δ-Al_2O_3 lattice because of the much lower efficiency in vacant sites occupation [17]. Moreover, divalent cations diffuse generally much more slowly at the given temperature than monovalent cations and their activation energy is also much larger. Thus, the preferential $MgAl_2O_4$ spinel compound formation we take to be unlikely here. The proposed model of interaction of Saffil fibres with liquid MgLi alloys is shown in Fig. 11.

The structural changes occurring in the described interaction course are characterized by the maintenance of the f c c oxygen anion sublattice involving only alterations to the octahedral cation sites occupation. As a result, the phase transformations towards $LiAl_5O_8$ are accomplished gradually, leading to the formation of a sequence of structurally coherent reaction products. From these interaction features it can be taken that no morphological changes of δ-Al_2O_3 crystallites occurred during their transformation towards $LiAl_5O_8$. A so-called topotactic phase transformation takes place here like that observed during boehmite (γ-AlOOH) transformation to the metastable transition alumina phases, which also is characterized by the O^{2-} spinel sublattice maintenance [6].

Obviously, the phase transformations accomplished in δ-Al_2O_3 crystallites during the course of their

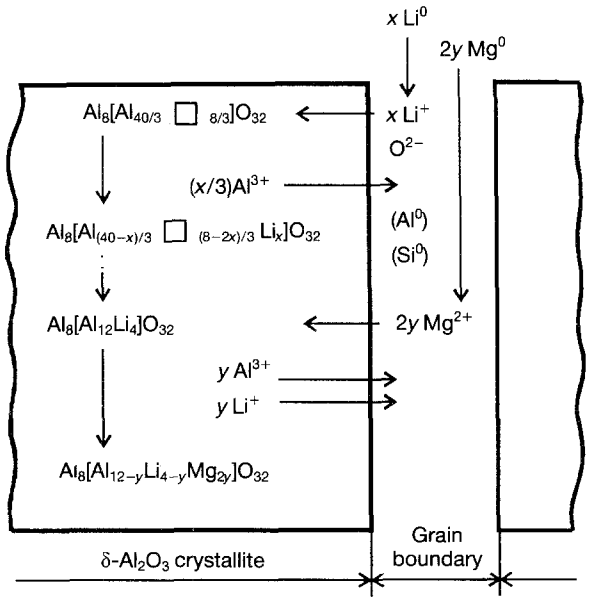

Figure 11 Proposed scheme of the interaction of Saffil fibres with MgLi alloys.

interaction with Li^+ cations, are not accompanied by induction of internal stresses, because of negligible volume changes as well as the above-mentioned structural coherence of the forming reaction products taking place here. Therefore, the experimentally observed tendency of Saffil fibres to embrittlement (Fig. 5) as a result of their interaction with MgLi alloys is not connected directly with the $LiAl_5O_8$ occurrence in Saffil fibres. In our opinion, this phenomenon is caused by the Li_2O accumulation at the δ-Al_2O_3 crystallite grain boundaries, where it is formed as an unavoidable reaction product preceding the $LiAl_5O_8$ spinel formation. The intergranular Li_2O is not coherent with the δ-Al_2O_3 lattice and, owing to considerable volume changes, will cause stresses and microcracks on the grain boundaries which explain the enhanced embrittlement of polycrystalline Saffil fibres.

5. Conclusions

1. In the infiltration of Saffil fibres with Mg8Li alloy, lithium penetrates the Saffil fibres at least to a depth of 100 nm and this process is accompanied by a gradual transformation of tetragonal δ-Al_2O_3 lattice towards spinel compound with a cell parameter of $a = 0.7934$ nm which is close to that reported for the $LiAl_5O_8$ spinel. The presence of magnesium in infiltrated Saffil fibres suggests the formation of mixed spinel of the $Al_8[Al_{12-x}Li_{4-x}Mg_{2x}]O_{32}$ type.

2. Neither a remarkable interfacial zone at the fibre/matrix interfaces nor other morphological changes of the Saffil fibres surface were observed; however, the Saffil fibres became brittle owing to interaction with the Mg8Li alloy which was manifested by the occurrence of fragmentation on the metallographically treated fibre cross-sections which correlated with the increase in infiltration temperature and infiltration time.

3. Areas of poorly infiltrated Saffil fibres were observed in the structure of prepared MMC. The maximum value of tensile strength $R_m = 225$ MPa corresponds to the minimum number of macrodefects (898 K/4 s). The tensile strength of the prepared MMC clearly decreased with increasing infiltration time.

References

1. D. A. WEIRAUCH and G. E. GRADDY, *J. Am. Ceram. Soc.* **75** (1992) 1484.
2. "JANAF Thermochemical Tables", 2nd Edn, US Department of Commerce NSRDS-NBS Vol. 37 (1971).
3. J. F. MASON, C. M. WARWICK, P. J. SMITH, J. A. CHARLES and T. W. CLYNE, *J. Mater. Sci.* **24** (1989) 3934.
4. Saffil Product Data Sheet, ICI, London (1984).
5. T. W. CLYNE, M. G. BADER, G. R. CAPPLEMAN and P. A. HUBERT, *J. Mater. Sci.* **20** (1985) 85.
6. S. J. WILSON and J. D. C. McCONNELL, *J. Solid State Chem.* **34** (1980) 315.
7. A. M. LEJUS and M. R. COLONGUES, *Compt. Rend. Acad. Sci.* **254** (1962) 2005.
8. L. E. DAVIS, N. C. MAC DONALD, P. W. PALMBERG, G. E. RIACH and R. E. WEBER, "Handbook of Auger Electron Spectroscopy", 2nd Edn (Physical Electronics Industries, Eden Prairie, 1976).
9. C. D. WAGNER, in "Practical Surface Analysis", Vol. 1, edited by M. P. Seah and D. Briggs (Wiley, Chichester, 1990) p. 595.
10. G. HANKE and K. MÜLLER, *Surf. Sci.* **152/153** (1985) 902.
11. H. HUGHES, R. D. BAXTER and B. PHILIPS, *IEEE Trans. Nucl. Sci.* **NS-19** (1972) 256.
12. D. J. TOWLE and C. M. FRIEND, *Mater. Sci. Technol.* **9** (1993) 35.
13. K. U. KAINER and B. L. MORDIKE, *Metall.* **44** (1990) 438.
14. B. HALLSTEDT, Z.-K. LIU and J. ÅGREN, *Mater. Sci. Eng.* **A129** (1990) 135.
15. B. C. LIPPENS and J. H. DE BOER, *Acta Crystallogr.* **17** (1964) 1312.
16. S. J. WILSON, *Proc. Br. Ceram. Soc.* **28** (1979) 281.
17. R. M. LEVY and D. J. BAUER, *J. Catal.* **9** (1967) 76.
18. E. KORDES, *Z. Kristallogr.* **91** (1935) 193.

Received 2 August 1993
and accepted 21 March 1994